Seismic vulnerability of steel tubular structures based on Local Buckling driving variables

Rúbia Bosse[1], Scarlet Montilla[2], Gustavo Gidrão[1], André Beck[3], Ricardo Picón[4], Julio Florez-Lopez[2].

[1]*Civil Engineering School, Federal University of Technology of Parana*
Rua Pres. Zacarias de Góes 875, 85053525, Guarapuava, Paraná, Brazil
rubiambosse@utfpr.edu.br, gidrao@utfpr.edu.br
[2]*School of Civil Engineering, Chongqing University*
No.174 Shazhengjie, Shapingba, 400045, Chongqing, China
scarlet.kmb03@gmail.com; j.florezlopez@cqu.edu.cn
[3]*São Carlos School of Engineering, University of São Paulo*
Avenida Trabalhador são-carlense, nº 400, 13566-590, São Carlos, Brazil.
atbeck@sc.usp.br
[4]*Departament of Civil Engineering and Geology, Catholic University of Temuco*
Araucanía, 3524040, Temuco, Chile
rpicon@uct.cl

Abstract. Performance-Based Earthquake Engineering (PBEE) is computationally demanding due to the multiple high-fidelity non-linear dynamic structural response analyses required to compute fragility curves. In this manuscript we propose an efficient procedure to obtain fragility curves of complex tubular structures, prone to fail due to local buckling, using a model based on the Lumped Damage Mechanics. A state variable characterizing local buckling is employed as engineering demand parameter (EDP) in PBEE. This state variable is a scalar, derived from lumped damage mechanics and taking values between 0 and 1, which characterizes the degree of local buckling (LB). A procedure to identify and define global collapse mechanisms using the failure probability maps based on the local buckling state variable is proposed. The identification of the elements controlling the occurrence of the failure mechanisms define which node should be used as the EDP for computing the structure's fragility curves. To evaluate the seismic vulnerability, incremental dynamic analyses are conducted. The main results demonstrate the efficiency of the mechanical model in a PBEE framework, and that the internal variables indicating local buckling can be considered objective indicators of collapse for Tubular complex steel frames. Results show how to identify the global failure mechanisms that are more likely to appear for each frame.

Keywords: Tubular Structures, Local Buckling, Lumped Damage Mechanics, Fragility Curves, Global Collapse Mechanism.

1 Introduction

The primary objective of Performance-based earthquake engineering (PBEE) is to evaluate and design structures that can achieve desired performance levels, presenting minimized damage, ensuring safety and reducing economic losses based on probabilistic assessments of seismic risk [1]. The PBEE framework is computationally intensive due to the need for numerous, highly accurate, nonlinear dynamic structural response analyses required to calculate fragility curves. Considering steel tubular structures in offshore environments, the occurrence of local buckling at the ends of the elements is often responsible for the damage and collapse of structures under high-intensity earthquake loading. Therefore, Lumped Damage Mechanics (LDM) models can be useful for probabilistic seismic analysis of complex tubular structures. LDM models are known for their combination of accuracy in the representation of non-linear material behavior and efficiency in the computation of dynamic structural response [8] [21]. This efficiency is crucial in PBEE formulations, given the necessity to account for record variability and uncertainties in system properties [1].

Some studies have simulated the collapse of tubular structures using finite element limit analysis and progressive collapse approaches under axial loads [2] [3]. In this paper, we propose the use of LDM to conduct

the structural analysis stage of PBEE from which will be derived fragility curves [4]. For the tubular steel structures, the LDM represents the evolution of driving rotation of damage and plasticity, lumped in inelastic hinges at the nodes of the elements, as internal variables. Practically, these internal state variables indicate local buckling occurrences at the nodes of steel tubular structures. The combination of several inelastic hinges representing local buckling under ground motion loads can lead to the formation of collapse mechanisms, resulting in the global failure of the system.

In this paper, we utilize Incremental Dynamic Analysis (IDA) to estimate the structural response of steel tubular frames and calculate fragility curves within a PBEE framework. Fragility curves describe the seismic vulnerability of structures, conditional on a given seismic intensity, and predefined limit states [5] [6] [7]. We propose the use of internal variables, such as driving rotation and damage, as Engineering Demand Parameters (EDPs) in the calculation of fragility curves. Traditional Probabilistic Seismic Demand Models (PSDMs) assuming lognormal distribution for structural analysis responses are not applicable to these variables. Hence, empirical estimation of failure probabilities is employed to define the seismic vulnerability of the structure, similar to methodologies used for reinforced concrete buildings [2].

The primary objective of this paper is to construct fragility curves for complex tubular structures using Incremental Dynamic Analysis (IDA) with Lumped Damage Mechanics (LDM). Additionally, this work proposes the use of failure probability maps, derived from the probability of each node exceeding predefined limit states at various seismic intensities. This method aims to identify and characterize damage leading to local buckling at element ends and to pinpoint collapse mechanisms in hyperstatic structures using system reliability theory.

2 Local buckling under mono-sign loads.

Consider a planar frame structure with three degrees of freedom at each node (Figure 1a). The displacement matrix is $\{\mathbf{u}\}^t_{\square} = (u_i, w_i, \theta_i, u_j, w_j, \theta_j)$. A state damage variable $\{D\}^t = (d_i, d_j)$ is introduced, where d_i-d_j are measures of the local buckling at the hinges i, j respectively (Figure 1b). The total generalized deformations of the element can be decomposed as [8]:

$$\{\mathbf{\Phi}\} = \{\mathbf{\Phi}^{\mathrm{e}}\} + \{\mathbf{\Phi}^{\mathrm{p}}\} + \{\mathbf{\Phi}^{\mathrm{d}}\} = [\mathbf{F(D)}]\{\mathbf{M}\} + \{\mathbf{\Phi}^{\mathrm{p}}\} + \{\mathbf{\Phi}^{\mathrm{d}}\}, \tag{1}$$

where $\mathbf{\Phi}^{\mathrm{e}}$ is the elastic beam-column deformation, $\mathbf{\Phi}^{\mathrm{p}}$ is the plastic rotations of the hinges and $\mathbf{\Phi}^{\mathrm{d}}$ damage rotations.

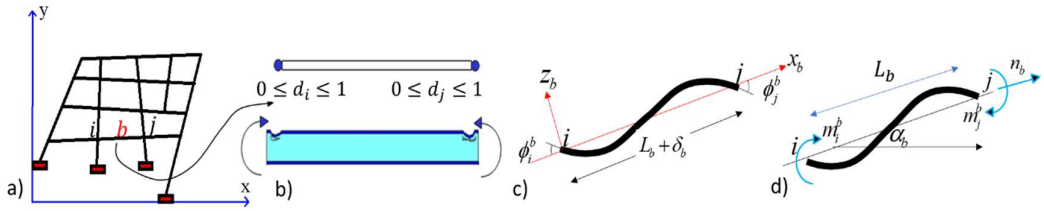

Figure 1. a) Representation of a frame b) Damage status of a frame member using a lumped inelasticity model, c) Generalized deformations of the member between the nodes *i* and *j* d) Generalized stresses.

The generalized stress matrix $\{\mathbf{M}\}^t_{\square} = (m_i^{\square}, m_j^{\square}, n)$ (Figure 1d), is the conjugate to the deformation matrix. It is composed of bending moments and axial force on the element. The matrix of nodal forces is defined as:

$$\{\mathbf{P}\} = [\mathbf{B}]^t_{\square}\{\mathbf{M}\}, \tag{2}$$

where $\{\mathbf{P}\}$ is the vector of internal forces, $[\boldsymbol{B}]$ is the transformation matrix and the superscript t is the transpose operator. The elasticity law is:

$$\{\mathbf{\Phi} - \mathbf{\Phi}^{\mathrm{p}}\}_b = [\mathbf{F(D)}]_{\mathrm{b}}\{\mathbf{M}\}_{\mathrm{b}} + \{\mathbf{\Phi}^0\}_{\mathrm{b}} \qquad [\mathbf{F(D)}] = \begin{bmatrix} \frac{L_b}{3(1-d_i)EI_b} & -\frac{L_b}{6EI_b} & 0 \\ -\frac{L_b}{6EI_b} & \frac{L_b}{3(1-d_j)EI_b} & 0 \\ 0 & 0 & \frac{L_b}{AE_b} \end{bmatrix} \tag{3}$$

where $[\mathbf{F(D)}]_{\mathrm{b}}$ is the flexibility matrix, L_b is the length of the element and EI_b is the bending stiffness, $\{\mathbf{\Phi}^0\}_{\mathrm{b}}$ is the initial strain vector of the element.

The evolution laws of a plastic hinge with local buckling are defined by:

$$\begin{cases}\dot{\phi}_i^p = 0 \;\; if \;\; f_i < 0 \\ f_i = 0 \;\; if \;\; \dot{\phi}_i^p \neq 0\end{cases}; \quad f_i = \left|\frac{m_i}{1-d_i}\right| - M_e(n) - \left(M_u(n) - M_e(n)\right)\left(1 - e^{-\beta|\phi_i^p|}\right)$$

$$\begin{cases}\dot{d}_\iota = 0 \;\; if \;\; |\phi_i^p| < R(d_i) \\ |\phi_i^p| = R(d_i) \;\; if \;\; \dot{d}_\iota > 0\end{cases}; \quad R(d_i) = p_{cr}(n) - \frac{1}{\kappa_m(n)}\ln\left(1 - \frac{d_i}{d_u}\right) \tag{4}$$

where the upper dot (.) represents derivative with respect to time, M_u and M_e are parameters of the yield function, d_u and κ_m are parameters of the damage function, and p_{cr} is the plastic rotation that initiates LB. The mechanical interpretation of model parameters is indicated in Figure 2. Constant β describes the plastic hardening rate. In compact sections, the plastic hardening phase has negligible influence on local buckling.

The local buckling evolution law is given in equation (5), as:

$$d_{i-j} = \kappa_m\langle p_{i-j} - p_{cr}\rangle; \qquad p_{i-j} = |\phi_{i-j}^p| \tag{5}$$

where p_{cr} is the critical plastic rotation that initiates local buckling and κ_m is the damage rate.

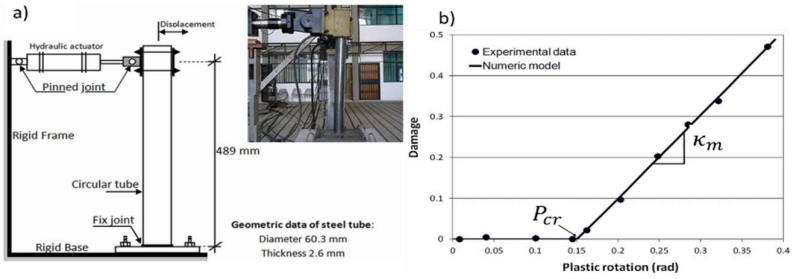

Figure 2. a) Monotonical test in a circular tube, b) Parameters of the damage evolution law.

3 Modelling local-buckling under cyclic loading

The elasticity law which describes unilateral behavior is given by:

$$\{\mathbf{\Phi} - \mathbf{\Phi^p}\} = [\mathbf{F}(n, \mathbf{D}^+)]\langle\mathbf{M}\rangle_+ + [\mathbf{F}(n, \mathbf{D}^-)]\langle\mathbf{M}\rangle_- \tag{6}$$

where the sets ($\mathbf{D}^+$) and ($\mathbf{D}^-$) correspond to the values of positive and negative LB, respectively; $\langle\mathbf{M}\rangle_+$ represents the positive part of matrix $\{\mathbf{M}\}$, i.e. $\langle m_i\rangle_+ = m_i$ if $m_i > 0$ and zero otherwise. $\langle\mathbf{M}\rangle_-$ is the negative part of $\{\mathbf{M}\}$: $\langle m_i\rangle_- = m_i$ if $m_i < 0$ and zero otherwise.

A yield function that also describes unilateral effect is:

$$f_i = Max\begin{cases} m_i - (1 - d_i^+)M_u(n) \\ -m_i + (1 - d_i^-)M_u(n)\end{cases} \tag{7}$$

The damage driving rotation (ddr) "Counter-buckling" is a phenomenon observed during cyclic loading. This effect, which occurs when the load changes sign, can be described as a process of "ironing out the wrinkles". In order to model the counter-buckling effect, the local buckling (LB) driving variables b_i^+, b_i^- are introduced:

$$\dot{b}_i^+ = \langle\dot{\phi}_i^p\rangle_+ + 0.6\,\langle\dot{\phi}_i^p\rangle_-; \; \dot{b}_i^- = -\langle\dot{\phi}_i^p\rangle_- - 0.6\,\langle\dot{\phi}_i^p\rangle_+ \tag{8}$$

where term $\langle\dot{\phi}_i^p\rangle_{+/-}$ represents again the positive/negative part of the plastic rotation rate. Notice that during the phases of positive bending moment ($\dot{\phi}_i^p > 0$) the LB driving variable $\dot{b}_i^+ = \dot{\phi}_i^p$ increases, i.e. positive LB is approaching or the "wrinkle" area is growing.

The damage evolution law is generalized to:

$$\begin{cases}\dot{d}_i^+ = 0 \;\; if \;\; b_i^+ < R(d_i^+) \\ b_i^+ = R(d_i^+) \;\; if \;\; \dot{d}_i^+ > 0\end{cases}; \qquad \begin{cases}\dot{d}_i^- = 0 \;\; if \;\; b_i^- < R(d_i^-) \\ b_i^- = R(d_i^-) \;\; if \;\; \dot{d}_i^- > 0\end{cases} \tag{9}$$

where function $R(\,)$ is the same of the mono-sign case. Notice that in the case of monotonic or mono-sign loadings, the damage evolution laws in Eqs. (9) and (4) give the same results.

The variables used as EDP for assessing the seismic vulnerability are the normalized LB driving rotations ddr^+, ddr^-. For a hinge i, they are defined as:

$$ddr_i^+ = \frac{b_i^+}{p_{cr}}; \qquad ddr_i^- = \frac{b_i^-}{p_{cr}} \tag{10}$$

p_{cr} is the initial LB resistance, local buckling initiation is defined by $ddr^{\pm} = 1$. Figure 3 shows the evolution of the local-buckling damage during an experimental cyclic test in a cantilever beam.

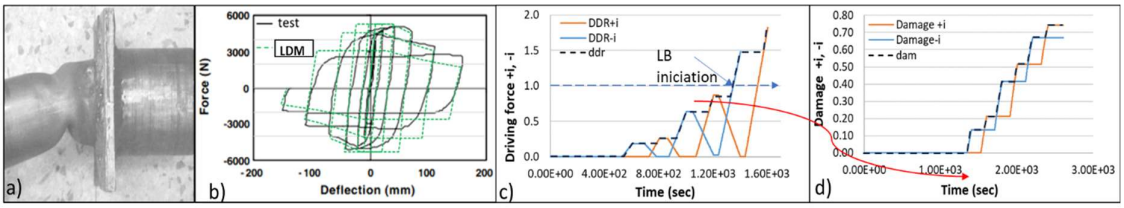

Figure 3. a) local buckling under cyclic loading b) force vs. deflection in a cantilever cyclic test; c) ddr evolution during the first 4 cycles of the simulation; d) damage evolution.

4 Fragility Analysis

In previous studies using internal variables derived from LDM in PBEE assessments it was verified that the damage variables resultant from the structural analysis under earthquakes do not follow log normal distribution, in this way, traditional PSDM approach that describe the fragility curves using analytical representations of the EDPs are not suitable [9] [10]. In this way, the fragility curves are calculated using traditional empirical method for each specific earthquake intensity, defined as:

$$P[EDP \geq C|IM] = \frac{m}{n} \tag{10}$$

where m is the number of simulations for which EDP's exceed a capacity limit C, and n is the total number of simulations for each earthquake intensity measure (IM). In this paper, three limit states are used: $ddr \geq 0.5$ indicating some plastic damage; $ddr \geq 1.00$ indicating the formation of an inelastic hinge; and $Dam \geq 0.99$ complete loss of stiffness due to LB. Where the Dam variable is defined as the maximum between positive and negative damages D$dam = Max(d^+, d^-)$,

5 Global collapse fragility curves

To obtain global collapse fragility curves, we identify the elements and their ends where local buckling (LB) first develops ($ddr \geq 1$) and determine the most likely sequence of LB failures by evaluating the sequence of nodes presenting the higher Pfs in the failure probability maps considering the limit states for each Intensity measure of the earthquakes. We then identify the most probable global collapse mechanism and the LB failures leading to it. In sequence we quantify the conditional probability of global collapse for each intensity measure. A global collapse mechanism corresponds to a parallel system of individual hinges forming the mechanism. The event "formation of a global collapse mechanism" (GC) can be described as:

$$GC = \bigcup_k \bigcap_{i \in S_k} LB_i \tag{11}$$

where LB_i represents local buckling at the i^{th} location (beam or column end), S_k is the set of indices for all LB events required to form the k^{th} mechanism, GC_k. The intersection ∩ represents a parallel combination of events, and the ∪ union represents a series system. Evaluating the probability of global collapse, $p_{GC} = P[GC]$, depends on the dependency between events in this equation. If failure sequences S_k are mutually exclusive, the probability is given by the sum of individual probabilities:

$$p_{GC} = P\left[\bigcup_k GC_k\right] = \sum_k P[GC_k] \tag{12}$$

Following Bosse et al [2], a strong correlation between individual LB events can help identify the single event (LB_{cr}) controlling the most likely failure sequence, given by eq. (13). In this approximation, p_{GC} includes all failure sequences ending with LB_{cr}, making it a practical method for assessing seismic vulnerability.

$$p_{GC} \approx P[GC_1] = P[\cap_{i \in S_k} LB_i] \approx P[LB_{cr}] \tag{13}$$

6 Results

6.1 Regular frame

The first example consists in an offshore structure represented in Figure 4a and Figure 4b. To perform IDA, a set of 30 earthquake signals were generated using the spectral representation method with the Clough-Penzien fully nonstationary power spectral density function [11] [12] [13] of a soil type C in Port Arthur, Texas, USA. The set of 30 earthquakes was specifically designed to provide a mean spectral acceleration response that matches the target response spectra prescribed by the American Standard [14] [15]. The modal analysis determined that the fundamental period was 0.92 s. Parameters $F_a = 1.3$, $F_v = 1.5$, $S_1 = 0.045$, $S_{MS} = 0.101$, $S_{M1} = 0.067$, $S_{DS} = 0.067$, $S_{D1} = 0.045$ and $T_L = 12$ s were employed to achieve the spectrum target response (Figure 4c).

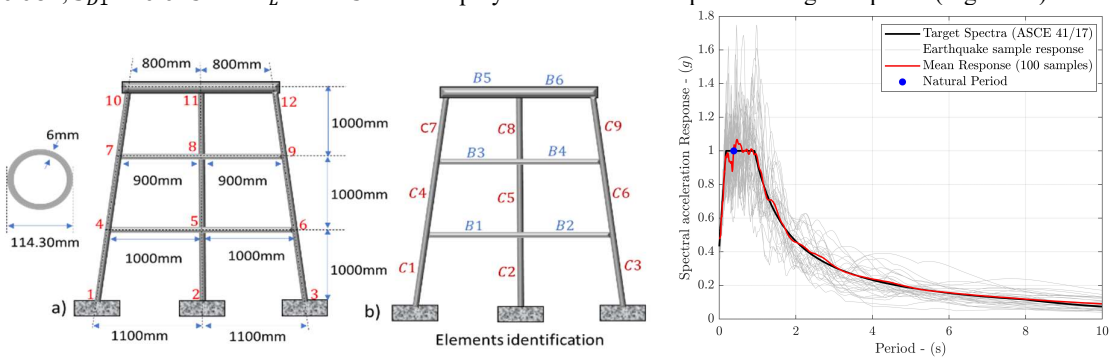

Figure 4 - Offshore structure b) Elements identification c) Spectral acceleration response of the spectrum-compatible generated earthquakes.

To identify the collapse mechanisms responsible for structural failure during earthquakes, we propose using failure probability maps. These maps illustrate the probability of each node in the structure exceeding a specified limit state related to the local buckling occurrence at various earthquake intensities. By analyzing these probability maps at progressively increasing intensities, we can pinpoint which nodes are the first to experience LB and which are the last. It is well-established that a hyperstatic frame can withstand a certain number of nodes undergoing LB; however, the cumulative effect of multiple nodes failing can trigger a local or global collapse mechanism. Figure 5 presents failure probability (P_f) maps for a intensity of $S_a = 2.0g$ for the three predefined limit states

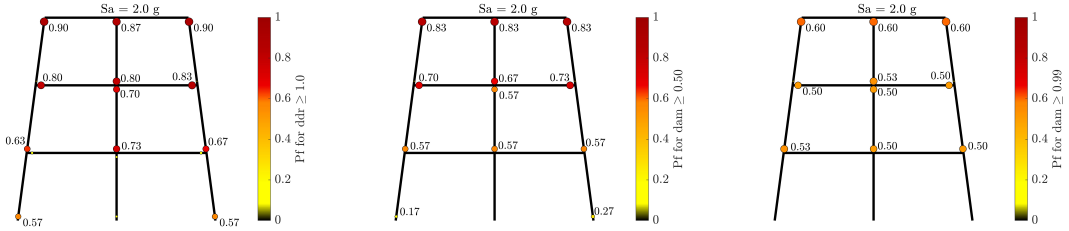

(a) (b) (c)

Figure 5 - Failure probability maps of the structure for three limit states at $S_a = 2.0g$.

The scale of $S_a = 2.0g$ was the final intensity tested on the structure. At this scale, some simulations did not reach convergence, indicating structural failure. Based on Figure 5, it can be observed that the top nodes of columns C7, C8, and C9 are the first to suffer LB, followed by the exterior nodes of beams B3 and B4, which show the highest Pf values across all limit states considered. When LB occurs at the base nodes of columns C4, C5, and C6, a collapse mechanism is triggered, causing the second and third floors of the frame to collapse, indicating a global failure of the structure. Thus, the base nodes of columns C4, C5, and C6 control the collapse mechanism occurrence at the structure. The collapse mechanism formation can be modeled as a parallel system. In such a system, the element with the lowest probability of failure (i.e., the strongest element) governs the occurrence of global failure. The application of system reliability theory to structural collapse has been previously studied [2].

The fragility curves representing the global failure of the structure can be derived using the internal

variables that describe the occurrence of local buckling as EDP at PBEE framework, particularly using the damage variables at the base nodes of columns C4, C5, and C6, which control the collapse mechanism. Figure 6 presents the fragility curves for three damage limit states: $ddr \geq 0.5$ indicating some plastic damage; $ddr \geq 1.00$ indicating the formation of an inelastic hinge; and $Dam \geq 0.99$ complete loss of stiffness due to LB. From Figure 6 it can be observed that the fragility curves of the three columns are similar with average Pfs for each limit state. The probability of a collapse mechanism formation is around 50% at the highest earthquake intensity tested. It can also be observed that the three curves of each limit state are close to each other, indicating that the accumulation of LB damage at the base of these columns occurs faster.

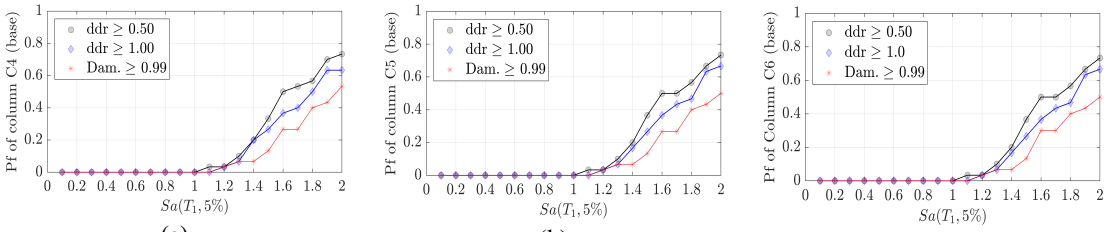

(a) (b) (c)

Figure 6. Fragility curves for the column C4, C5 and C6 Global failure.

6.2 Irregular Frame

Figure 7 illustrates the second example, a structural configuration of an irregular frame. Figure 8 presents failure probability (P_f) maps for a intensity of $S_a = 1.5g$, the highest tested in the frame. These maps consider the following limit states: damage driving rotation, $ddr \geq 1$ indicating the onset of damage accumulation in the nodes; damage variable, $dam \geq 0.5$ indicating the occurrence of LB with 50% of a damage; and damage variable, $dam \geq 0.99$, indicating complete loss of stiffness due to LB.

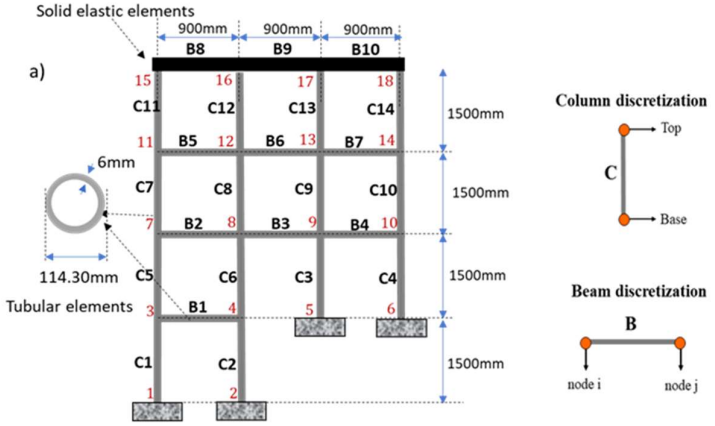

Figure 7. Irregular frame

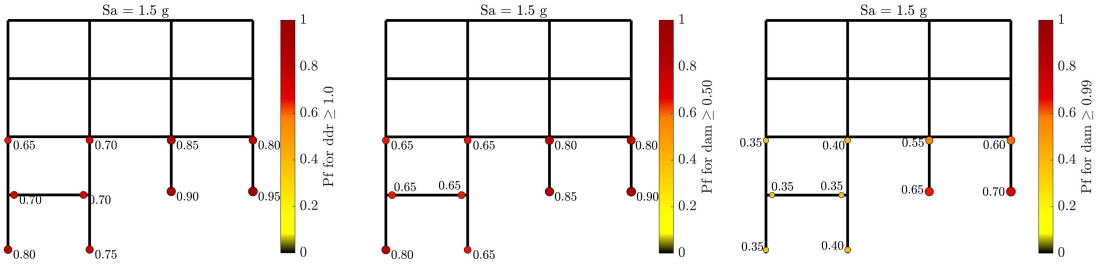

a) b) c)

Figure 8 – Failure probability maps of the structure for three limit states at $S_a = 1.5g$.

Based on Figure 5, it can be observed that the base nodes of columns C3 and C4 are the first to suffer LB,

followed by the top nodes of these columns (with the highest Pfs in all frame). In this case it can be observed that these are the first elements to fail, representing a local failure to the frame, in which the frame will still stay standing. When LB occurs at the top nodes of columns C5 and C6 and at both node of beam B1, a collapse mechanism is triggered, causing the first and second floors of the frame to collapse, indicating a global failure of the structure. Thus, the top nodes of columns C5, and C6 and the nodes of beam B1 are indicated to be the nodes that control the collapse mechanism occurrence at the structure.

The fragility curves representing the global failure of the structure can be derived using the internal variables indicating LB of top nodes of C5, C6 and B1 as EDP. Figure 9 presents the fragility curves for three damage limit states: $ddr \geq 0.5$ indicating some plastic damage; $ddr \geq 1.00$ indicating the formation of an inelastic hinge; and $Dam \geq 0.99$ complete loss of stiffness due to LB. From Figure 9 it can be observed that the three elements present similar fragility curves. The probability of a complete collapse mechanism formation is around 40% at the highest earthquake intensity tested.

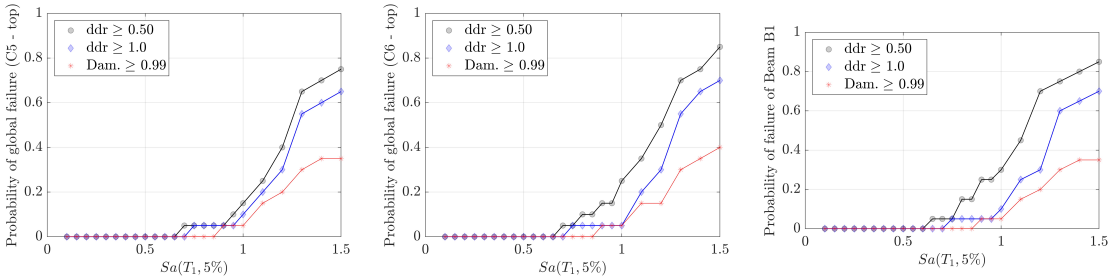

(a) (b) (c)

Figure 9. Fragility curves for the columns C5, C6 and beam B1.

7 Conclusions

In this paper, we propose the use of Lumped Damage Model (LDM) to model local buckling (LB) of tubular steel structures for seismic vulnerability assessment. The LDM incorporates internal variables, such as the driving damage rotation (ddr) and the damage variable (dam), which capture stiffness and strength degradation during load-unload cycles and represent local buckling events. Key findings include: (a) ddr and dam are effective indicators of local buckling and stiffness loss, which aid in the identification of global collapse mechanisms in hyperstatic frame structures under seismic loading; (b) the LDM approach demonstrated acceptable accuracy and computational efficiency in assessing seismic fragility, but requires calibration against experimental results or higher fidelity FE models; (c) The probability of failure maps facilitated the identification and evaluation of LB failure sequences leading to global collapse mechanisms, which can guide optimal design approaches for asymmetric tubular frames under seismic actions.

References

[1] H.-K. D. V. T. N. D.-K. T. Sy Hung Mai, "Stochastic nonlinear inelastic analysis for steel frame structure using Monte Carlo sampling," *Ain Shams Engineering Journal,* vol. 14, no. 11, p. 102527, 2023.

[2] K.-P. K. H. S. K. Hoon Huh, "Collapse simulation of tubular structures using a finite element limit analysis approach and shell elements," *International Journal of mechanical Sciences,* vol. 43, no. 9, pp. 2171-2187, 2001.

[3] Y. Z. F. G. Jie Song, "A relationship between progressive collapse and initial buckling for tubular structures under axial loading," *International Journal of Mechanical Sciences,* vol. 75, pp. 200-211, 2013.

[4] S. K. B. Y. L. J. P. R. E. M. F.-L. J. Montilla Barrios, "Multi-scale analysis of life-cycle corrosion damages in steel tubular structures subjected to earthquake loading," in *18th International Symposium on Tubular Structures*, Beijing, China, 2023.

[5] F. E. M. A. FEMA-274, "NEHRP Commentary on the guidelines for the seismic rehabilitation of buildings," FEDERAL EMERGENCY MANAGEMENT AGENCY, Washington, D.C, 1997.

[6] FEMA-302, *Recommended Provisions for the Development of Seismic Regulations for New Buildings: FEMA 302;,* Washington D.C.: National Earthquake Hazard Reduction Program, Building Seismic Safety Council, Federal Emergency Management Agency, 1997.

[7] FEMA-P-58-6, *Guidelines for Performance-Based Seismic Design of Buildings,* Redwood City, California: Report prepared by the Applied Technology Council for the Federal Emergency Management Agency, 2018.

[8] Flórez-López, R. Picón and M. Marante, Fracture and Damage Mechanics for Structural Engineering of Frames: State-of-the-Art Industrial, Hershey PA, United States of America: IGI Global, 2015.

[9] B. Sudret and C. V. Mai, "Computing derivative-based global sensitivity measures using polynomial chaos expansions," *Reliability Engineering & System Safety,* vol. 134, pp. 241-250, 2014.

[10] M. Xiong and Y. Huang, "Static and dynamic reliability analysis of laterally loaded pile using probability density function method," *Journal of Marine Science and Engineering,* vol. 8, no. 12, p. 994, 2020.

[11] P. Cacciola, "A stochastic approach for generating spectrum compatible fully nonstationary earthquakes," *Computers and Structures,* vol. 88, no. 15-16, pp. 889-901, 2010.

[12] Cacciola and G. Deodatis, "A method for generating fully non-stationary and spectrum-compatible ground motion vector processes," *Soil Dynamics and Earthquake Engineering,* vol. 31, no. 3, pp. 351-360, 2011.

[13] D. L. Z. I. Cacciola P., "New insights in the analysis of the structural response to response-spectrum-compatible accelerogram," *Engineering Structures,* vol. 78, pp. 3-16, 2014.

[14] ACI-318, "Building Code Requirements for Structural Concrete.," p. 524 p., 2014.

[15] ASCE/SEI-41-17, *Seismic Evaluation and Retrofitof Existing Buildings,* Reston, Virginia: American Society of Civil Engineers, 2017.

[16] J. B. A. F.-L. J. Bazán, "Random fatigue of plane frames via lumped damage mechanics," *Engineering Structures,* vol. 182, pp. 301-315, 2019.

[17] L. E. F.-L. J. Coelho K., "An efficient mechanical-probabilistic approach for the collapse modelling of RC structures," *Ibracom Structures and Materials Journal,* vol. 12, no. 2, pp. 386-397, 2019.

[18] K. L. E. F.-L. J. Coelho, "A methodology to evaluate corroded RC structures using a probabilistic damage approach," *Computers and Concrete,* vol. 29, no. 1, pp. 1-14, 2022.

[19] K. R. K. &. R. B. Porter, "Creat-ing fragility functions for performance-based earthquake engineering," *Earthquake Spectra,* vol. 23, no. 2, pp. 471-489, 2007.

[20] I. Zentner, M. Gündel and N. Bonfils, "Fragility analysis methods: Review of existing approaches and application," *Nuclear Engineering and Design,* pp. 245-258, 2017.

[21] R. Bosse, J. Flórez-López, G. Gridão, I. Rodrigues and A. Beck, "Collapse mechanisms and fragillity curves based on Lumped damage Mechanics for RC frames subjected to earthquakes," *Engineering Structures,* vol. 311, p. 118115, 2024.

[22] M. Shinozuka and G. Deoadatis, "Stochastic process models for earthquake ground," *Probabilistic Engineering Mechanics,* vol. 3, no. 3, p. 114–123, 1988.

[23] Deodatis, "Non-stationary stochastic vector processes : seismic ground motion," *Probabilistic Engineering Mechanics, v. 11,* p. 149–168, 1996.

[24] P. Cacciola and I. Zentner, "Generation of response-spectrum-compatible artificial earthquake accelerograms with random joint time – frequency distributions," *Probabilistic Engineering Mechanics,* pp. 52-58, 2012.

[25] M. G. Flenga and M. Favvata, "Probabilistic seismic assessment of the pounding risk based on the local demands of a multistory RC frame structure," *Engineering Structures,* vol. 245, p. 112789, 2021.

[26] T. Rossetto and A. Elnashai, "Derivation of vulnerability functions for European-type RC structures based on observational data," *Engineering Structures,* vol. 25, no. 10, pp. 1241-1263, 2003.